Materials Chemistry and Physics 322 (2024) 129524

Contents lists available at ScienceDirect

Materials Chemistry and Physics

journal homepage: www.elsevier.com/locate/matchemphys

Fe_3O_4/Au nanocomposites: Characterization and cytotoxicity effects in vitro

R.N. Yaroslavtsev [a,b,*], A.V. Tyumentseva [a], D.A. Velikanov [b], I.G. Vazhenina [b], M.N. Volochaev [b], S.V. Stolyar [a,b]

[a] Krasnoyarsk Science Center, Federal Research Center KSC SB RAS, Akademgorodok 50, Krasnoyarsk, 660036, Russia
[b] Kirensky Institute of Physics, Federal Research Center KSC SB RAS, Akademgorodok 50, bld. 38, Krasnoyarsk, 660036, Russia

HIGHLIGHTS

- Magnetic nanocomposites of Fe_3O_4/Au were synthesized.
- Magnetic properties of nanoparticles were studied using magnetometry and FMR.
- Magnetic Fe_3O_4/Au particles can reduce metabolic activity of living cells.
- Fe_3O_4/Au nanocomposites affect the mRNA level of SOD1 and GPX1 genes.

ARTICLE INFO

Keywords:
Magnetic nanoparticles
Magnetite
Gold nanoparticles
Cytotoxicity

ABSTRACT

Magnetic nanocomposites containing iron oxide and gold components take great attention last years because of their relative biocompatibility and the ability to combine the magnetic properties of iron and the chemical bonding properties of gold for the possible drug delivery or diagnostics for various diseases. However, such particles have some toxicity to living cells, and the effect depends on many factors, including size, shape, the ratio of components in the composites, and the type of cells affected. And thus, the search for compositions and technologies for producing iron-gold particles with improved properties and reduced cytotoxicity remains relevant. The aim of the study was to synthesize and characterize Fe_3O_4/Au nanocomposites and evaluate their influence on living cells using the example of cell line HEK293.

Fe_3O_4 nanoparticles (NPs) were synthesized by co-precipitation of Fe^{2+}/Fe^{3+} water solution in alkaline conditions and then boiled with $HAuCl_4$ in 0.1 M sodium citrate. The NPs properties were estimated by transmission electron microscopy (TEM), vibration magnetometry and ferromagnetic resonance (FMR).

According to magnetometric measurements, nanoparticles are mainly in a superparamagnetic state. By fitting magnetization curves, the magnetic characteristics of nanoparticles were determined: saturation magnetization (59.3 emu/g) and magnetic anisotropy constant ($K = 0.86 \cdot 10^5$ erg/cm^3). The average particle size estimated from magnetic measurements was 8.7 nm. Considering the presence of a magnetically dead layer, this is in good agreement with the TEM results. The temperature dependence of the FMR linewidth was analyzed using two models. As a result, the parameters $M_S V$ and K/M_S were determined. The models used showed good agreement. The values of the anisotropy constant ($K = 1.06 \cdot 10^5$ erg/cm^3) and the average particle size (6.8 nm) are estimated.

The effect of the NPs on the HEK293 cells was studied by MTT-assay, flow cytometry and RT-PCR. The exposure with the NPs lead to a significant decrease of cell metabolic activity in HEK293 cell culture, but this effect was not accompanied by cell death. It was shown that the expression of antioxidant enzymes SOD1 and GPX1 was reduced at the mRNA stage. So the NPs synthesized may affect gene expression and metabolism of HEK293 cells, but this does not have fatal consequences for cell viability.

* Corresponding author. Krasnoyarsk Science Center, Federal Research Center KSC SB RAS, Akademgorodok 50, Krasnoyarsk, 660036, Russia.
E-mail address: yar-man@bk.ru (R.N. Yaroslavtsev).

https://doi.org/10.1016/j.matchemphys.2024.129524
Received 29 January 2024; Received in revised form 8 May 2024; Accepted 29 May 2024
Available online 4 June 2024

1. Introduction

Composite materials based on magnetite and gold nanoparticles (NPs) are widely used for bio- and nanotechnologies. Due to the relative biocompatibility of Fe_3O_4 and Au, they are considered dual-use materials (therapeutic and diagnostic). In recent years, a huge number of fluorescent markers, vector molecules and drugs have been developed for the functionalization of Fe_3O_4/Au [1–4].

One of the most important characteristics of NPs for biomedical applications is their cytotoxicity [5]. This allows us to assess how much the potential benefit of using magnetic particles for the intended purpose exceeds the harm caused to a living object. Since gold in its bulk state has high chemical stability and low toxicity, gold NPs were initially thought to be excellent for biomedical applications. However, subsequent studies indicate that when nano-sized gold is used, in addition to its physicochemical parameters, its ability to influence living objects also changes, manifested in increased cytotoxicity [6–8]. To reduce the toxic effect, as well as to impart magnetic properties to gold particles, they are studied in composites with magnetic metals, the most biocompatible among which is iron oxide [9]. In such a compound, iron oxide imparts magnetic properties to the composite, and gold atoms provide useful optical properties, as well as catalytic activity and surface effects [10–12].

Development and research of NPs containing Au atoms show different toxicity results in in vitro and in vivo models. They suggest that the cytotoxicity of gold NPs depends on many factors, including their own properties (size, shape, concentration, presence of a shell on the surface), the method of delivering them to the body, and the type of cells affected. Thus, in Ref. [13], a multiparametric assessment of the cytotoxicity of Au NPs with a diameter of 4 nm coated with polymethacrylic acid was performed. The authors used multiple cell types, different nanoparticle concentrations and incubation times, and different toxicity assessment methods. The final noncytotoxic concentration was determined to be 10 nM. At higher concentrations, a decrease in cell viability and cytoskeletal deformation was observed. The paper [14] presents a toxicity study of 13.5 nm gold NPs in mice. Low concentrations of gold NPs do not cause apparent loss of body weight or noticeable toxicity. High concentrations of gold NPs caused a decrease in body weight, red blood cells and hematocrit. Of the three routes of administration, the oral and intraperitoneal routes showed the highest toxicity, and tail vein injection showed the lowest toxicity. The authors of [15] studied the cytotoxicity of AuNPs of various forms and with different surface chemical compositions (cetyltrimethylammonium bromide (CTAB), poly(ethylene glycol) (PEG) and human serum albumin (HSA)). The authors of [16] showed that the cytotoxicity of gold NPs depended primarily on their size, and not on the chemical composition of the ligands (excluding CTAB which was toxic for the cells). The 1–2 nm particles were significantly more toxic than the larger 15 nm gold colloids, regardless of the cell type tested.

Thus, to date, there is no consensus regarding the cytotoxicity of gold NPs. And therefore, the search for new options and methods for the synthesis of nanocomposites containing Au atoms, which have less cytotoxicity is still relevant.

The most effective way to reduce any possible toxicity of nanoparticles is to coat them with a dense inert material (usually a polymer) [17,18]. However, if it is necessary to use the surface properties or catalytic activity of gold, this method is not applicable. Therefore, there is a need for an in-depth study of the mechanisms of interaction of Au or Fe/Au nanocomposites with living cells and biological molecules to understand possible side effects and be able to control the action of the NPs. The purpose of this study was to synthesize magnetic particles containing iron and gold atoms, to study their physicochemical properties, as well as the features of their effect on a living cell in the absence of a coating.

2. Experimental

2.1. Synthesis of Fe_3O_4/Au nanocomposites

Fe_3O_4 magnetic NPs were obtained by co-precipitation from a solution of $FeCl_3 \cdot 6H_2O$ and $FeCl_2 \cdot 4H_2O$ salts in a molar ratio of 2:1 at room temperature. 0.17 g of iron (II) chloride and 0.46 g of iron (III) chloride were dissolved in 100 ml of distilled water with stirring. After complete dissolution of the salts, 2.5 ml of NH_4OH (25 %) was added to the solution. Stirring was continued for 30 min. After the completion of the reaction, the magnetic NPs were collected with a magnet and washed several times in distilled water to pH = 7.0. The preparation of the Fe_3O_4/Au composite was performed as follows. 0.5 ml of a suspension of Fe_3O_4 NPs with a concentration of 20 mg/ml was added to a 1 M sodium citrate solution with a volume of 100 ml. Bring the solution to a boil. Then 0.25 ml of 0.2 M $HAuCl_4$ solution was added. Boiling was continued for 15 min.

2.2. Characterization of nanocomposites

Electron microscopic studies were carried out on a Hitachi HT7700 transmission electron microscope (accelerating voltage 100 kV). UV–Vis absorbance spectra were measured on a SPECTROstar Nano plate spectrometer (BMG Labtech, Germany). Ferromagnetic resonance (FMR) spectra were measured with the X-band (9.4 GHz) spectrometer ELEXSYS E580 (Bruker, Germany). The static magnetic measurements were performed on an automated vibrating sample magnetometer in fields of up to 15 kOe at room temperature. The studies were carried out on the equipment of the Krasnoyarsk Regional Center of Research Equipment of Federal Research Center « Krasnoyarsk Science Center SB RAS».

2.3. Cell culture

Human embryonic kidney cell line HEK-293 (ATCC CRL-1573) was kindly provided by Shemyakin-Ovchinnikov Institute of Bioorganic Chemistry of the Russian Academy of Sciences (Russia). The cells were grown in Dulbecco's Modified Eagles' Medium (DMEM) (Gibco, USA) with 10 % of fetal bovine serum (Himedia, South America) and non-essential amino-acids (Paneco, Russia) at 37 °C and 5 % CO_2.

2.4. MTT assay

The cells were seeded in two 96-well plates at the concentration $1 \cdot 10^5$ cells per mL ($1.5 \cdot 10^3$ cells per well) and incubated for 24 h for cells attaching. Then culture medium was replaced to the same with addition of magnetic NPs Fe_3O_4/Au at concentrations 0, 50, 100, 200 and 400 mg/L in each plate. The samples were further incubated, and cell viability/metabolic activity was evaluated at 24 and 48 h. For this purpose, at a preassigned time point culture medium was replaced in one of the plates to the medium with 0.5 ml/mL MTT reagent. Then the cells were incubated for 2 h for MTT reduction to formazan in living cells. Further culture medium was carefully discarded and the cells were lysed in DMSO and formazan was dissolved. OD_{560} was measured by spectrophotometer SpectroStar Nano (BMG Labtech, Germany) and was proportional to the metabolic activity of the culture. According to studies, gold NPs may have catalytic activity similar to that of some enzymes [19,20]. To exclude the possible spontaneous reduction of MTT to formazan in the presence of the NPs from the calculations, additional controls were introduced into the experiment. They contained the NPs in appropriate concentrations, but not containing living cells. The optical density of the solution in these wells was subtracted from the data of the experimental sample with the corresponding concentration of the NPs in the cell culture.

2.5. Flow cytometry

To estimate the effect of the NPs on cell death by apoptosis or necrosis in the cell culture flow cytometry was performed using Caspase 3/7 kit (BioRad, USA). HEK293 cells were prepared as upper described and incubated with the NPs at the concentration 50 mg/L for 48 h. Then the cells were harvested and stained with PI and Caspases 3/7 antibodies according to manufacturer's instruction.

2.6. RT-PCR

RT-PCR is one of the most accurate and convenient methods that is widely used to assess molecular changes in cells [21,22]. It allows the assessment of gene expression at the post-transcriptional level.

HEK293 cells were incubated with the Fe_3O_4/Au NPs (50 mg/L) for 48 h and then RNA was isolated from the cells using HiPure RNA Kit (Magen, China). Reverse transcription was performed with OT-M-MuLV-RH kit (Biolabmix, Russia) according to manufacturer's protocol. CAT and SOD1 genes were chosen as targets for gene expression analysis, and two endogenous controls were used for data normalizing: ACTB and GAPDH. HS-qPCR kit (Biolabmix, Russia) was used to prepare PCR mixture with the addition of 400 nmol of each primer and 350 nmol of fluorescent probe per reaction. The cDNA was added to the reaction cocktail at 10 % of mixture volume.

2.7. Statistical analysis

All biological experiments were carried out in five replicates and non-parametric statistics were applied to their analysis. The data presented as medians and upper and lower quartiles.

Relative expression levels of CAT and SOD1 genes were calculated by ddCt method [23]. Pared comparisons of treated and control samples were performed with Mann-Whitney non-parametric *U* test.

3. Results and discussion

3.1. Characterization of nanocomposites

High-resolution transmission electron microscopy (HRTEM) images of Fe_3O_4 NPs and Fe_3O_4/Au nanocomposite are shown in Fig. 1a and Fig. b. The average size of the magnetite core is 9.8 ± 1.8 nm (Fig. 1c). The polydispersity index calculated as σ/d was equal to 0.18. This polydispersity value indicates fairly good uniformity in particle size. The microdiffraction pattern of the Fe_3O_4 sample (inset in Fig. 1a) has reflections characteristic of the magnetite spinel structure. The Fe_3O_4/Au sample has a (111) peak in the microdiffraction pattern corresponding to fcc-Au (inset in Fig. 1b). The energy-dispersive x-ray (EDX) spectrum (Fig. 1d) also confirms the presence of gold in the sample. The optical density spectrum of the nanocomposites (Fig. 1e) contains a peak at ~520 nm, due to the plasmon resonance of gold NPs.

The magnetization curves (Fig. 2) were measured in the field range from −15 to 15 kOe and in the temperature range from 80 to 300 K. They are symmetrical to zero field and contain reversible and irreversible parts, i.e., a hysteresis loop. The coercive force, remanent magnetization, and magnetization in a field of 15 kOe decrease with increasing temperature. The coercive field values indicate that particles of this size are close to the superparamagnetic state. The low values of the saturation magnetization of the nanocomposite compared to bare magnetite nanoparticles are due to gold inclusions.

The fitting of the magnetization curves was carried out using a function representing the sum of Akulov's law and the Langevin function:

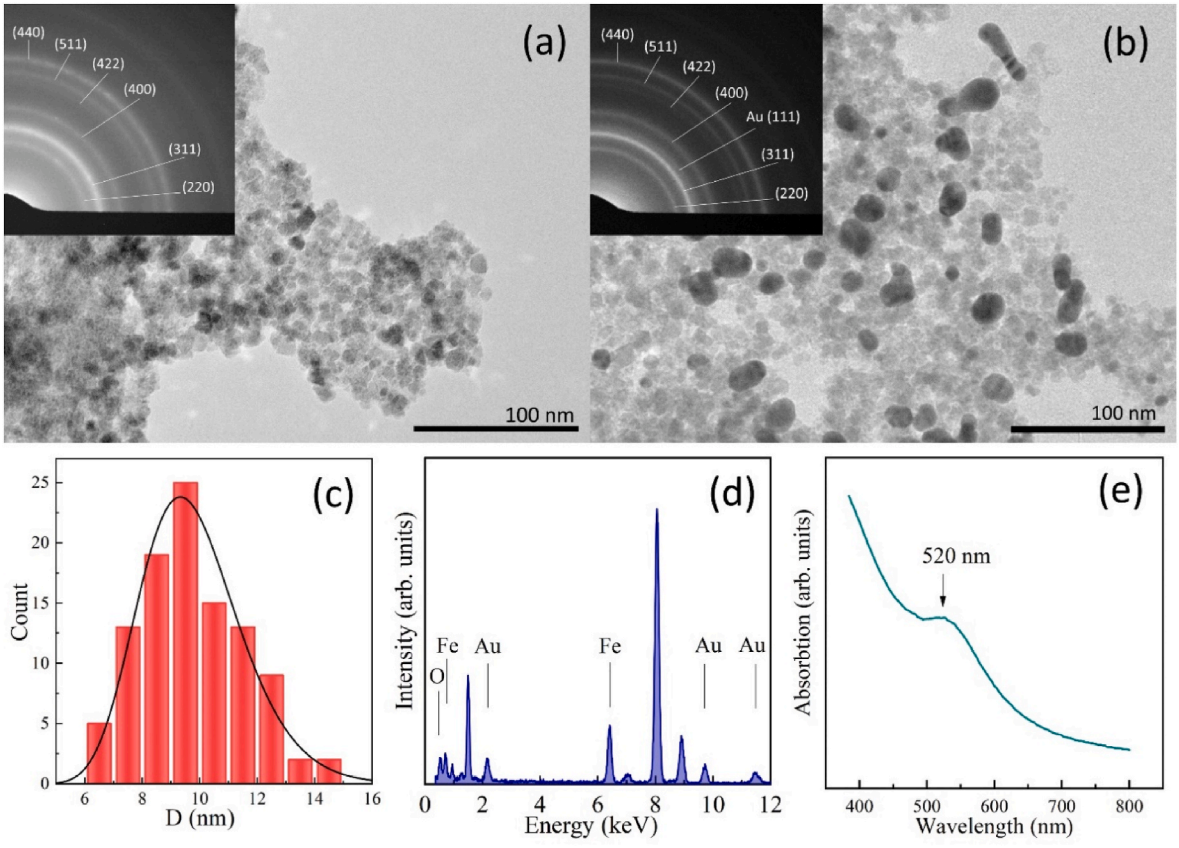

Fig. 1. (a) HRTEM image of Fe_3O_4, (b) HRTEM image of Fe_3O_4/Au nanocomposite, (c) size distribution of Fe_3O_4 particles, (d) EDX spectrum of Fe_3O_4/Au, (e) optical density spectrum of Fe_3O_4/Au.

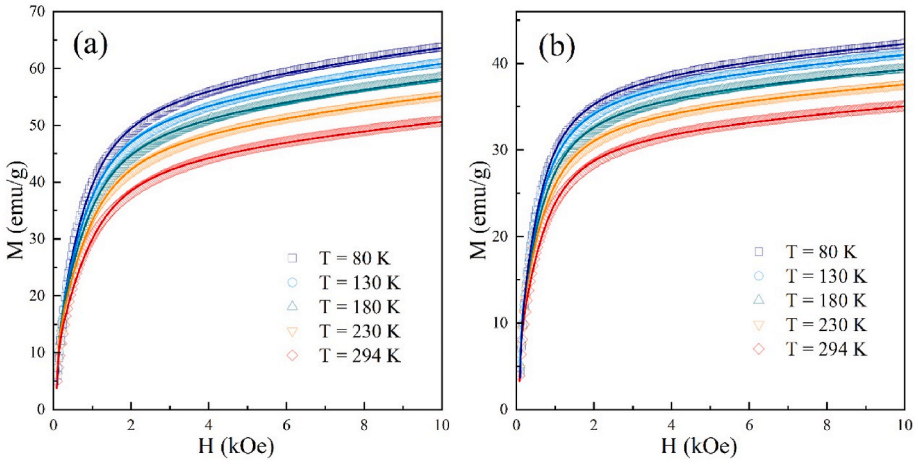

Fig. 2. The magnetization curves of Fe_3O_4 (a) and Fe_3O_4/Au (b).

$$M(H) = xM_S\left(1 - \left(\frac{aH_a}{H}\right)^2\right) + (1-x)M_S\left(\coth\left(\frac{H\mu_P}{kT}\right) - \frac{kT}{H\mu_P}\right) + \chi H \quad (1)$$

where M_S is the saturation magnetization, x is the ratio between Akulov's law and the Langevin function, μ_P is the average magnetic moment of the particle, χ is the contribution from the spin glass shell, characteristic of iron oxide nanoparticles. $H_a = 2K/M_{S0}$ is the field of local magnetic anisotropy, K is the energy of local magnetic anisotropy of particles, and a is the coefficient due to the symmetry of magnetic anisotropy equal to $(2/105)^{1/2}$ for cubic magnetic anisotropy.

Approximation of the measured $M(H)$ dependencies made it possible to find the saturation magnetization M_S, average magnetic moment of the particle μ_P and the local magnetic anisotropy field H_a (Table 1).

The saturation magnetization M_S decreases with increasing temperature and is described by the Bloch's law:

$$M_S(T) = M_{S0}\left(1 - B \bullet T^{3/2}\right) \quad (2)$$

Fitting the experimental data with this function made it possible to determine the values of the Bloch constant and the saturation magnetization (Fig. 3). The Bloch constant for the Fe_3O_4 sample was $4.4{\cdot}10^{-5}$ $K^{-3/2}$, which correlates well with other studies [24,25].

The resulting saturation magnetization value (59.3 emu/g) differs from bulk magnetite (92 emu/g). The decrease in saturation magnetization with decreasing size is explained by the spin-glass layer on the surface of the particles and is observed experimentally in many studies [24,26].

The relationship between Akulov's law and the Langevin function can be interpreted as the relationship between particles in blocked and unblocked states. In our case, it was 0.2, i.e., most nanoparticles are in an unblocked superparamagnetic state, and the average blocking temperature lies below the studied range (below 80 K).

Table 1
Magnetic characteristics of NPs.

	M_S, emu/g	H_a, Oe	μ_P, emu
Fe_3O_4			
80 K	57.79	764.6	$2.65{\cdot}10^{-17}$
130 K	55.13	677.5	$4.07{\cdot}10^{-17}$
180 K	52.90	627.5	$5.44{\cdot}10^{-17}$
230 K	50.26	593.3	$6.70{\cdot}10^{-17}$
294 K	46.27	570.1	$8.27{\cdot}10^{-17}$
Fe_3O_4/Au			
80 K	39.65	686.4	$3.50{\cdot}10^{-17}$
130 K	38.48	558.7	$5.54{\cdot}10^{-17}$
180 K	36.99	551.5	$7.10{\cdot}10^{-17}$
230 K	35.22	544.1	$8.98{\cdot}10^{-17}$
294 K	32.84	511.1	$11.08{\cdot}10^{-17}$

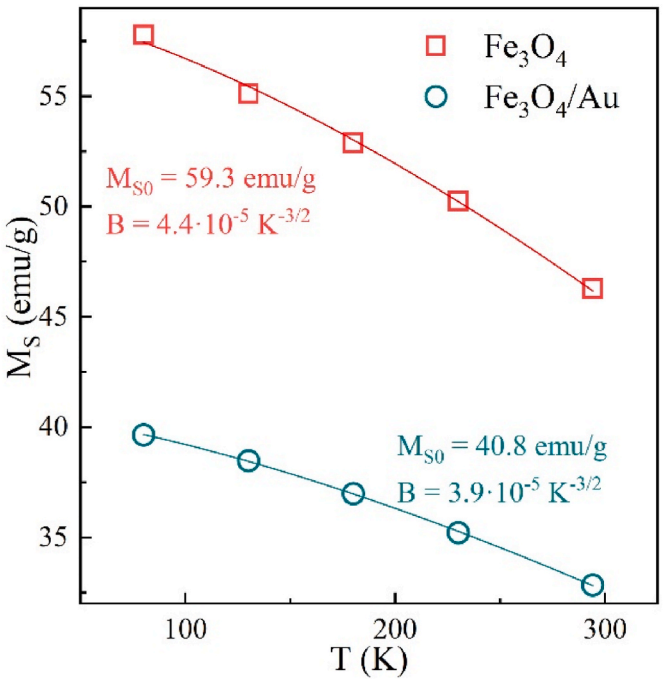

Fig. 3. Temperature dependencies of saturation magnetization as well as fitting by Eq. 2.

Using data obtained from fitting magnetization curves, we can calculate the following characteristics: the ratio between magnetite and gold in the sample, the magnetic anisotropy constant K, and the average magnetite particle size. Using the saturation magnetization of Fe_3O_4 ($M_{S0} = 59.3$ emu/g) and Fe_3O_4/Au ($M_{S0} = 40.8$ emu/g) we can calculate the ratio between gold and magnetite in the sample: 31.2 % of Au. The magnetic anisotropy constant calculated as $K = M_{S0}{\cdot}H_a/2$ was $0.86{\cdot}10^5$ erg/cm^3. Typically, in magnetite nanoparticles the K value is in the range of $1–2{\cdot}10^5$ erg/cm^3. Using the value of the average magnetic moment μ_P, the average particle size can be calculated. Assuming that the nanoparticles have a spherical shape, the average particle size was 8.7 nm. The difference between the obtained size and electron microscopy data is due to a disordered layer on the surface that does not participate in magnetic resonance.

The FMR of the obtained nanocomposite was measured in the tem-

perature range of 60–280 K (Fig. 4). The values of the resonance field, linewidth, and integral intensity were calculated from the spectra, the temperature dependencies of which are shown in Fig. 4b, c, d. The value of the resonant field is close to the value of ω/γ and slowly decreases with decreasing temperature.

The temperature dependence of the integrated intensity is non-monotonic and has a maximum (~200 K), which can be interpreted as a transition of NPs to the superparamagnetic state [27]. The blocking temperature is determined by the Neel-Brown relation $\ln(\tau/\tau_0) = KV/k_BT$. Here τ_0 is the particle relaxation time, and τ is the characteristic time which is determined by the measurement method. For the magnetometry method, τ is ~10 s, for the FMR method $\tau \sim 10^{-10}$ s. Thus, the ratio between the blocking temperatures obtained by these two methods will be $T_B^{M(T)} \approx T_B^{FMR}/4$ [28]. $T_B^{M(T)}$ estimated in this way is ~50 K, which is consistent with magnetometric data.

To analyze the temperature dependence of the FMR linewidth, we used two models [29,30].

According to the first theory [31,32], the absorption line width Δ H(T) is determined by the sum of two contributions: the contribution due to the superparamagnetism of NPs (ΔH_S) and the contribution due to the spread in the directions of particle anisotropy fields (ΔH_U).

$$\Delta H(T) = \Delta H_S(T) + \Delta H_U(T) = \frac{\alpha\omega(\xi - L_1)}{\sqrt{3}\xi\gamma L_1} + 3\frac{K}{M_S}\frac{L_2}{L_1} \quad (1)$$

where M_S is the magnetization, ω is the frequency, γ is the gyromagnetic ratio, K is the anisotropy constant, $\alpha = 0.01$ is the damping parameter, $L_{1,2}$ are the Langevin functions.

$$L_1 = \coth x - \frac{1}{\xi}, L_2 = 1 - \frac{3L_1}{\xi} \quad (2)$$

$\Delta H_S(T)$ and $\Delta H_U(T)$ are functions of the Langevin parameter $\xi = \frac{\omega M_S V}{\gamma kT}$, where V is the volume of the particle, k is the Boltzmann constant, T is the temperature.

The fitting results are shown in Fig. 5. M_SV and K/M_S were used as fitting parameters, which were $3.7 \cdot 10^{-17}$ emu and 340 Oe, respectively.

According to the second model [29,33], the apparent superparamagnetic anisotropy field H_{SP} is determined by the following relation:

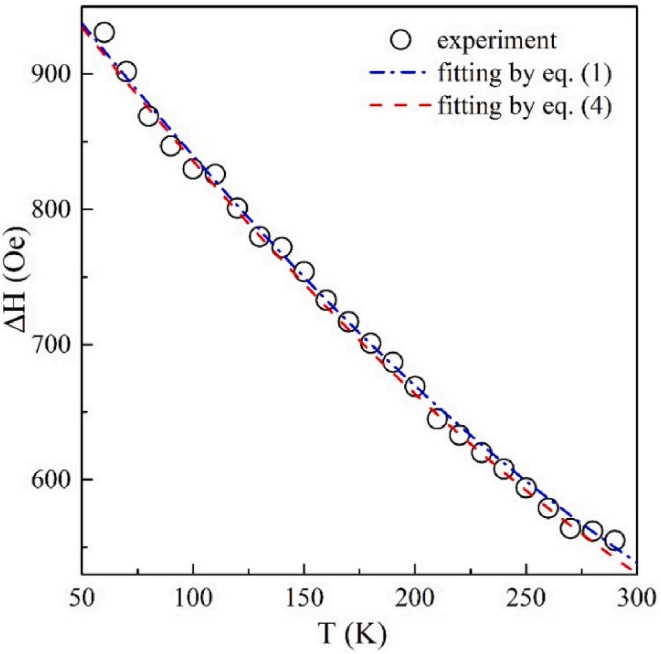

Fig. 5. Temperature dependence of the FMR linewidth and fitting results.

$$H_{SP} = H_{bulk}\frac{\left(1 - 3\xi^{-1}\cot h\xi + 3\xi^{-2}\right)}{\cot h\xi - \xi^{-1}} \quad (3)$$

where ξ – Langevin parameter, H_{bulk} – bulk anisotropy field,

The value of H_{SP}, according to Ref. [34] can be represented as $H_{SP} = 2\Delta H/3$. Thus, equation (3) is rewritten as follows:

$$\Delta H(T) = \frac{3K}{M_S}\frac{\left(1 - 3\xi^{-1}\cot h\xi + 3\xi^{-2}\right)}{\cot h\xi - \xi^{-1}} \quad (4)$$

For this model, M_SV and K/M_S were also used as fitting parameters (the values of the best fit were $M_SV = 3.95 \cdot 10^{-17}$ emu and $K/M_S = 350$ Oe).

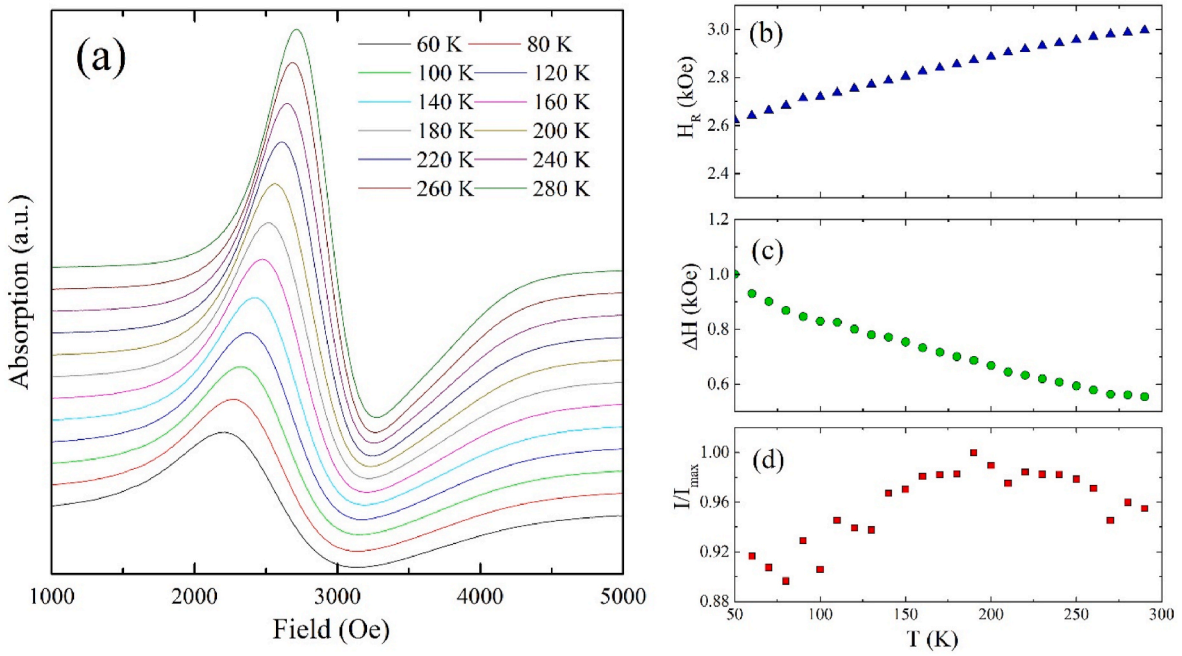

Fig. 4. (a) FMR spectra, temperature dependences of (b) resonance field, (c) linewidth, and (d) integrated intensity.

The obtained values from two different models are in good agreement. Using the magnetization value of bare magnetite NPs, obtained from magnetometric data, the values of the anisotropy constant and nanoparticle size were calculated. The anisotropy constant was $1.06 \cdot 10^5$ erg/cm^3. The average nanoparticle size, assuming a spherical shape, was 6.8 nm. The obtained values of the anisotropy constant and the average particle size are close to the values obtained from magnetometric data.

3.2. Fe_3O_4/Au NPs effects on living cells HEK293

Gold NPs cytotoxicity was demonstrated in many studies [35,36]. We observed dose dependent effect of our NPs on HEK293 cells, though it wasn't linear (Fig. 6). Cell metabolic activity was decreased to 50.8 % even at 50 mg/L of the NPs in the culture medium after 24 h of incubation, and retained at the similar level when the particles' concentration was increased. After 48 h, minimal cell metabolism was observed at 100 mg/L of the NPs (26.6 %). It should be noted that according to studies (and our observations on another cell lines) a concentration of iron oxide particles of 50 mg/L does not have a significant influence on cell metabolism [37,38]. Thus, we believe that the effect we observed was due to the presence of gold components. It is shown that IC50 of Au NPs may be less than 5 mg/L in some shapes [39]. In our experiments Au ratio was about 31.2 %, and thus we have Au concentration range from 15 to 120 mg/L, and it was in the complex with iron oxide. These amounts may be large enough to demonstrate significant inhibiting, but it doesn't explain the absence of further decrease of metabolic activity when NPs concentration grows from 50 to 400 mg/L.

The results of flow cytometry assessing the proportion of living, dead and apoptotic cells made it possible to clarify that the drop in metabolic activity in the culture was not caused by cell death. It was shown that the proportion of living cells in the control sample was 93.04 %, and in the sample after incubation with the NPs – 92.06 % (Fig. 7). According to the literature, gold NPs are able to inhibit enzymes activity in the cell [40,41]. So in our study, gold NPs probably suppressed the activity of the enzymes that reduce MTT to formazan, but did not cause cell death in the culture. Moreover, we suppose that Au inhibits a specific group of

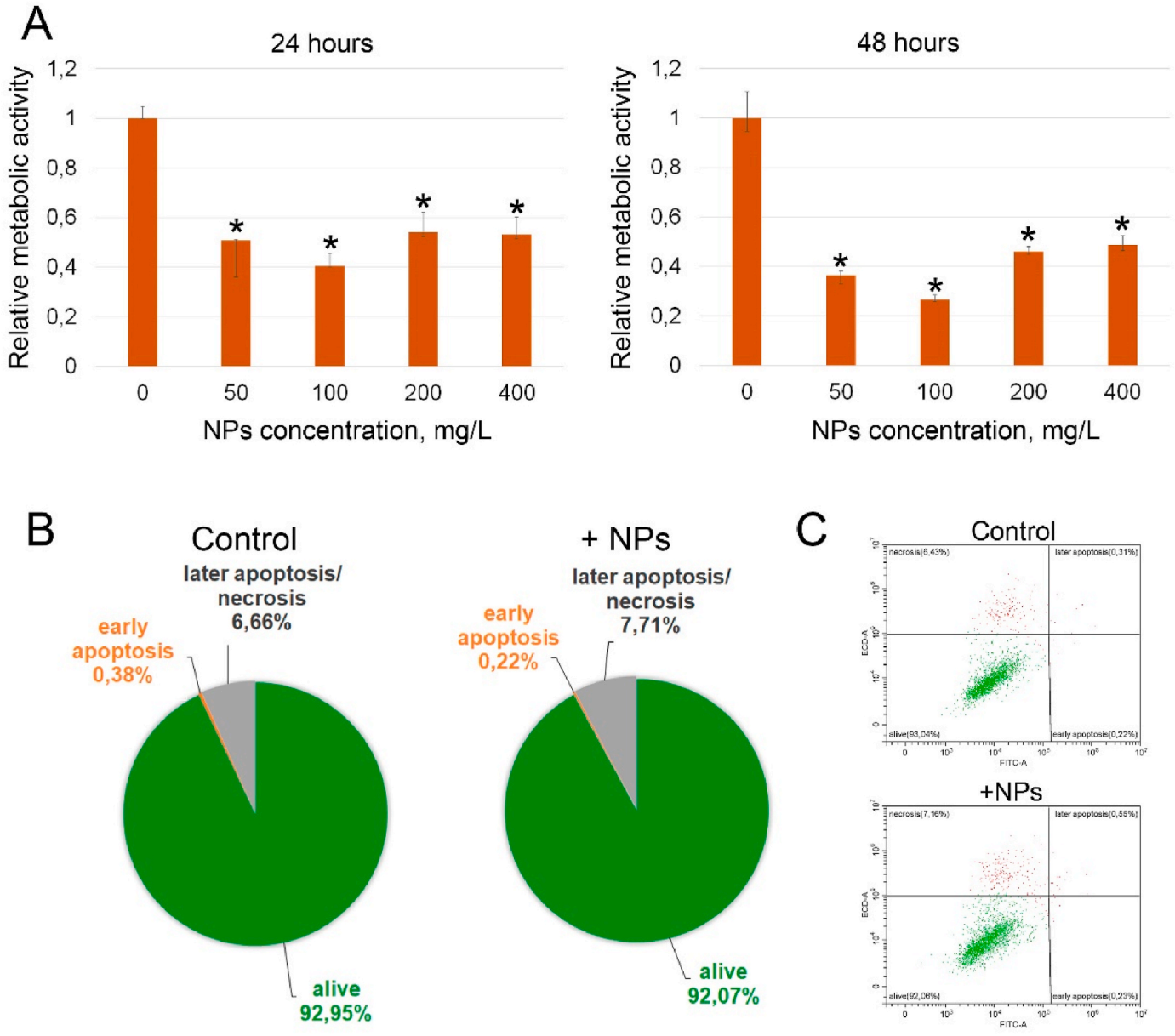

Fig. 6. Fe_3O_4/Au NPs effect on HEK293 cells. A - metabolic activity changes in the cell cultures after 24 and 48 h incubation with the NPs at different concentrations (MTT assay). B – Caspase test results obtained by flow cytometry; C – Examples of cell distribution in caspase test.

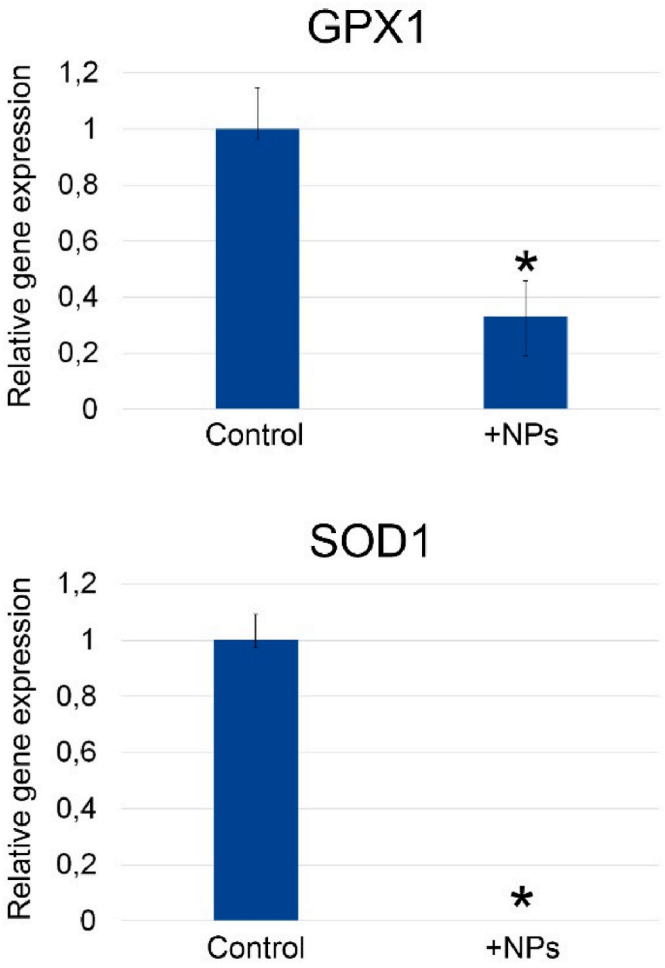

Fig. 7. *GPX1* and *SOD1* gene expression alterations under the influence of 50 mg/L Fe_3O_4/Au NPs (48 h of exposure).

enzymes without affecting others. In this case, achieving a certain concentration of gold particles leads to the suppression of the activity (or synthesis) of all enzymes that it is capable of regulating, and a further increase in the amount of this metal in the medium does not entail an increase in the effect. At the same time, the work of other enzymes remains unaffected, and this ensures the vital activity of cells. But this hypothesis requires confirmation.

Iron oxide NPs are known to be able to cause oxidative stress in living cells [42,43] so it was expected that NPs contact with HEK293 cells may increase expression of the genes encoding antioxidant enzymes *SOD1* and *GPX1*. Further we tried to evaluate the influence of Fe_3O_4/Au complexes on the expression of these genes. RT-PCR results demonstrated a significant decrease in the expression of the *GPX1* gene, encoding glutathione peroxidase 1, to 33 % of the control, while the level of *SOD1* gene mRNA became undetectable. It allows to assume that a decrease of enzymes activity by Au NPs may be caused by the interference of gold in the synthesis of the enzyme at the transcriptional or post-transcriptional level of gene expression. Our results are consistent with the study of Yang Y. and colleagues who demonstrate that gold NPs influence gene expression profiles in dermal fibroblasts and significant changes affected genes associated with the regulation of metabolism and gene transcription [44].

4. Conclusion

Thus, magnetic NPs were obtained that combine iron oxide and gold. Characterization of nanocomposites by FMR, TEM and magnetometry methods made it possible to determine magnetic parameters such as saturation magnetization, coercivity and magnetic anisotropy constant. The effect of particles of this composition on living cells is manifested in the suppression of metabolism, including through the regulation of the expression of genes *SOD1* and *GPX1* encoding the antioxidant enzymes. Such exposure does not entail cell death, but requires careful study of the mechanisms to improve the biosafety of particles.

Our study has some limitations because it assessed only one ratio of iron and gold atoms in the particle composition. We do not exclude that changing this ratio may change the effects on living objects. However, our study can be compared with work studying the effect of pure iron oxide on the cell, and our data indicate a difference in the effect, which is obviously caused by the presence of gold atoms.

Funding

This study was carried out within the State Assignment for the "Krasnoyarsk Science Center", Siberian Branch of the Russian Academy of Sciences.

CRediT authorship contribution statement

R.N. Yaroslavtsev: Writing – review & editing, Writing – original draft, Visualization, Investigation, Data curation, Conceptualization. **A. V. Tyumentseva:** Writing – review & editing, Writing – original draft, Visualization, Investigation, Data curation, Conceptualization. **D.A. Velikanov:** Investigation. **I.G. Vazhenina:** Investigation. **M.N. Volochaev:** Investigation. **S.V. Stolyar:** Writing – review & editing, Supervision, Resources, Project administration, Conceptualization.

Declaration of competing interest

The authors declare that they have no known competing financial interests or personal relationships that could have appeared to influence the work reported in this paper.

Data availability

Data will be made available on request.

References

[1] H.K. Patra, S. Banerjee, U. Chaudhuri, P. Lahiri, A.K. Dasgupta, Cell selective response to gold nanoparticles, Nanomed. Nanotechnol. Biol. Med. 3 (2007) 111–119, https://doi.org/10.1016/j.nano.2007.03.005.
[2] X. Lv, Z. Fang, Y. Sun, Y. Yang, X. Wang, Y. Chen, Y. Qin, N. Li, C. Li, J. Xu, H. Bao, Interfacial preparation of multi-branched magneto-plasmonic Fe3O4@Au core@shell nanocomposites as efficient photothermal agents for antibacterial application, J. Alloys Compd. 932 (2023) 167712, https://doi.org/10.1016/j.jallcom.2022.167712.
[3] Z. Izadiyan, K. Shameli, S.-Y. Teow, M. Yusefi, P. Kia, E. Rasouli, M.A. Tareq, Anticancer activity of 5-fluorouracil-loaded nanoemulsions containing Fe3O4/Au core-shell nanoparticles, J. Mol. Struct. 1245 (2021) 131075, https://doi.org/10.1016/j.molstruc.2021.131075.
[4] Y. Xue, B. Karmakar, J. Ke, H.A. Ibrahium, N.S. Awwad, A.F. El-kott, Immobilized Au nanoparticles on chitosan-biguanidine modified Fe3O4 nanoparticles and investigation of its anti-human lung cancer activity, J. Saudi Chem. Soc. 26 (2022) 101391, https://doi.org/10.1016/j.jscs.2021.101391.
[5] M. Kus-Liśkiewicz, P. Fickers, I. Ben Tahar, Biocompatibility and cytotoxicity of gold nanoparticles: recent advances in methodologies and regulations, Int. J. Mol. Sci. 22 (2021) 10952, https://doi.org/10.3390/ijms222010952.
[6] A. Sani, C. Cao, D. Cui, Toxicity of gold nanoparticles (AuNPs): a review, Biochem. Biophys. Reports. 26 (2021) 100991, https://doi.org/10.1016/j.bbrep.2021.100991.
[7] E. Caballero-Díaz, M. Valcárcel, Toxicity of Gold Nanoparticles, 2014, pp. 207–254, https://doi.org/10.1016/B978-0-444-63285-2.00005-5.
[8] Y.-P. Jia, B.-Y. Ma, X.-W. Wei, Z.-Y. Qian, The in vitro and in vivo toxicity of gold nanoparticles, Chin. Chem. Lett. 28 (2017) 691–702, https://doi.org/10.1016/j.cclet.2017.01.021.
[9] M.A.M. Tarkistani, V. Komalla, V. Kayser, Recent advances in the use of iron–gold hybrid nanoparticles for biomedical applications, Nanomaterials 11 (2021) 1227, https://doi.org/10.3390/nano11051227.

[10] J. Lou-Franco, B. Das, C. Elliott, C. Cao, Gold nanozymes: from concept to biomedical applications, Nano-Micro Lett. 13 (2021) 10, https://doi.org/10.1007/s40820-020-00532-z.
[11] X. Bai, Y. Wang, Z. Song, Y. Feng, Y. Chen, D. Zhang, L. Feng, The basic properties of gold nanoparticles and their applications in tumor diagnosis and treatment, Int. J. Mol. Sci. 21 (2020) 2480, https://doi.org/10.3390/ijms21072480.
[12] M.C. Daniel, D. Astruc, Gold nanoparticles: assembly, supramolecular Chemistry, quantum-size-related properties, and applications toward biology, catalysis, and nanotechnology, Chem. Rev. 104 (2004) 293–346, https://doi.org/10.1021/cr030698+.
[13] S.J. Soenen, B. Manshian, J.M. Montenegro, F. Amin, B. Meermann, T. Thiron, M. Cornelissen, F. Vanhaecke, S. Doak, W.J. Parak, S. De Smedt, K. Braeckmans, Cytotoxic effects of gold nanoparticles: a multiparametric study, ACS Nano 6 (2012) 5767–5783, https://doi.org/10.1021/nn301714n.
[14] X. Zhang, H. Wu, D. Wu, Y. Wang, J. Chang, Z. Zhai, A. Meng, P. Liu, L. Zhang, F. Fan, Toxicologic effects of gold nanoparticles in vivo by different administration routes, Int. J. Nanomed. 771 (2010), https://doi.org/10.2147/IJN.S8428.
[15] M. Bhamidipati, L. Fabris, Multiparametric assessment of gold nanoparticle cytotoxicity in cancerous and healthy cells: the role of size, shape, and surface Chemistry, Bioconjugate Chem. 28 (2017) 449–460, https://doi.org/10.1021/acs.bioconjchem.6b00605.
[16] Y. Pan, S. Neuss, A. Leifert, M. Fischler, F. Wen, U. Simon, G. Schmid, W. Brandau, W. Jahnen-Dechent, Size-dependent cytotoxicity of gold nanoparticles, Small 3 (2007) 1941–1949, https://doi.org/10.1002/smll.200700378.
[17] O. Baber, M. Jang, D. Barber, K. Powers, Amorphous silica coatings on magnetic nanoparticles enhance stability and reduce toxicity to in vitro BEAS-2B cells, Inhal. Toxicol. 23 (2011) 532–543, https://doi.org/10.3109/08958378.2011.592869.
[18] N. Malhotra, J.-S. Lee, R.A.D. Liman, J.M.S. Ruallo, O.B. Villaflores, T.-R. Ger, C.-D. Hsiao, Potential toxicity of iron oxide magnetic nanoparticles: a review, Molecules 25 (2020) 3159, https://doi.org/10.3390/molecules25143159.
[19] Y. Zhang, S. Li, H. Liu, W. Long, X.-D. Zhang, Enzyme-like properties of gold clusters for biomedical application, Front. Chem. 8 (2020), https://doi.org/10.3389/fchem.2020.00219.
[20] W. He, Y.-T. Zhou, W.G. Wamer, X. Hu, X. Wu, Z. Zheng, M.D. Boudreau, J.-J. Yin, Intrinsic catalytic activity of Au nanoparticles with respect to hydrogen peroxide decomposition and superoxide scavenging, Biomaterials 34 (2013) 765–773, https://doi.org/10.1016/j.biomaterials.2012.10.010.
[21] S.A.S. Shandiz, M. Khosravani, S. Mohammadi, H. Noorbazargan, A. Mirzaie, D. N. Inanlou, M.D. Jalali, H. Jouzaghkar, F. Baghbani-Arani, B. Keshavarz-Pakseresht, Evaluation of imatinib mesylate (Gleevec) on KAI1/CD82 gene expression in breast cancer MCF-7 cells using quantitative real-time PCR, Asian Pac. J. Trop. Biomed. 6 (2016) 159–163, https://doi.org/10.1016/j.apjtb.2015.10.006.
[22] A. Moshfegh, A. Salehzadeh, S.A. Sadat Shandiz, M. Shafaghi, A.S. Naeemi, S. Salehi, Phytochemical analysis, antioxidant, anticancer and antibacterial properties of the caspian sea red macroalgae, laurencia caspica, Iran, J. Sci. Technol. Trans. A Sci. 43 (2019) 49–56, https://doi.org/10.1007/s40995-017-0388-5.
[23] K.J. Livak, T.D. Schmittgen, Analysis of relative gene expression data using real-time quantitative PCR and the 2−ΔΔCT method, Methods 25 (2001) 402–408, https://doi.org/10.1006/meth.2001.1262.
[24] S.V. Komogortsev, S.V. Stolyar, L.A. Chekanova, R.N. Yaroslavtsev, O.A. Bayukov, D.A. Velikanov, M.N. Volochaev, P.E. Eroshenko, R.S. Iskhakov, Square plate shaped magnetite nanocrystals, J. Magn. Magn Mater. 527 (2021) 167730, https://doi.org/10.1016/j.jmmm.2021.167730.
[25] G.F. Goya, T.S. Berquó, F.C. Fonseca, M.P. Morales, Static and dynamic magnetic properties of spherical magnetite nanoparticles, J. Appl. Phys. 94 (2003) 3520–3528, https://doi.org/10.1063/1.1599959.
[26] A.P. Safronov, I.V. Beketov, S.V. Komogortsev, G.V. Kurlyandskaya, A.I. Medvedev, D.V. Leiman, A. Larrañaga, S.M. Bhagat, Spherical magnetic nanoparticles fabricated by laser target evaporation, AIP Adv. 3 (2013) 052135, https://doi.org/10.1063/1.4808368.
[27] I.G. Vazhenina, S.V. Stolyar, A.V. Tyumentseva, M.N. Volochaev, R.S. Iskhakov, S. V. Komogortsev, V.F. Pyankov, E.D. Nikolaeva, Study of magnetic iron oxide nanoparticles coated with silicon oxide by ferromagnetic method, Phys. Solid State 65 (2023) 884, https://doi.org/10.21883/PSS.2023.06.56095.01H.
[28] S.V. Stolyar, S.V. Komogortsev, A.S. Gorbenko, Y.V. Knyazev, R.N. Yaroslavtsev, I. A. Olkhovskiy, D.S. Neznakhin, A.V. Tyumentseva, O.A. Bayukov, R.S. Iskhakov, Maghemite nanoparticles for DNA extraction: performance and blocking temperature, J. Supercond. Nov. Magnetism 35 (2022) 1929–1936, https://doi.org/10.1007/s10948-022-06233-5.
[29] R.S. de Biasi, A.A.R. Fernandes, Ferromagnetic resonance evidence for superparamagnetism in a partially crystallized metallic glass, Phys. Rev. B 42 (1990) 527–529, https://doi.org/10.1103/PhysRevB.42.527.
[30] Y.L. Raikher, V.I. Stepanov, Thermal fluctuation effect on the ferromagnetic-resonance line-shape in disperse ferromagnets, J. Exp. Theor. Phys. Lett. 102 (1992) 1409–1423.
[31] I.S. Poperechny, Y.L. Raikher, Ferromagnetic resonance in uniaxial superparamagnetic particles, Phys. Rev. B 93 (2016) 014441, https://doi.org/10.1103/PhysRevB.93.014441.
[32] S.V. Stolyar, R.N. Yaroslavtsev, A.V. Tyumentseva, S.V. Komogortsev, E. S. Tyutrina, A.T. Saitova, Y.V. Gerasimova, D.A. Velikanov, M.V. Rautskii, R. S. Iskhakov, Manifestation of stoichiometry deviation in silica-coated magnetite nanoparticles, J. Phys. Chem. C 126 (2022) 7510–7516, https://doi.org/10.1021/acs.jpcc.2c00349.
[33] E. Wajnberg, L.J. El-Jaick, M.P. Linhares, D.M.S. Esquivel, Ferromagnetic resonance of horse spleen ferritin: core blocking and surface ordering temperatures, J. Magn. Reson. 153 (2001) 69–74, https://doi.org/10.1006/jmre.2001.2430.
[34] D.L. Griscom, Ferromagnetic resonance spectra of lunar fines: some implications of line shape analysis, Geochem. Cosmochim. Acta 38 (1974) 1509–1519, https://doi.org/10.1016/0016-7037(74)90171-9.
[35] S.K. Surapaneni, S. Bashir, K. Tikoo, Gold nanoparticles-induced cytotoxicity in triple negative breast cancer involves different epigenetic alterations depending upon the surface charge, Sci. Rep. 8 (2018) 12295, https://doi.org/10.1038/s41598-018-30541-3.
[36] S. Vijayakumar, S. Ganesan, In vitro cytotoxicity assay on gold nanoparticles with different stabilizing agents, J. Nanomater. 2012 (2012) 1–9, https://doi.org/10.1155/2012/734398.
[37] C. Costa, F. Brandão, M.J. Bessa, S. Costa, V. Valdiglesias, G. Kiliç, N. Fernández-Bertólez, P. Quaresma, E. Pereira, E. Pásaro, B. Laffon, J.P. Teixeira, In vitro cytotoxicity of superparamagnetic iron oxide nanoparticles on neuronal and glial cells. Evaluation of nanoparticle interference with viability tests, J. Appl. Toxicol. 36 (2016) 361–372, https://doi.org/10.1002/jat.3213.
[38] S. Kanagesan, M. Hashim, S. Tamilselvan, N.B. Alitheen, I. Ismail, A. Hajalilou, K. Ahsanul, Synthesis, characterization, and cytotoxicity of iron oxide nanoparticles, Adv. Mater. Sci. Eng. 2013 (2013) 1–7, https://doi.org/10.1155/2013/710432.
[39] K.P. Steckiewicz, E. Barcinska, A. Malankowska, A. Zauszkiewicz–Pawlak, G. Nowaczyk, A. Zaleska-Medynska, I. Inkielewicz-Stepniak, Impact of gold nanoparticles shape on their cytotoxicity against human osteoblast and osteosarcoma in in vitro model. Evaluation of the safety of use and anti-cancer potential, J. Mater. Sci. Mater. Med. 30 (2019) 22, https://doi.org/10.1007/s10856-019-6221-2.
[40] Y. Huang, J. Jiang, Y. Wang, J. Chen, J. Xi, Nanozymes as enzyme inhibitors, Int. J. Nanomed. 16 (2021) 1143–1155, https://doi.org/10.2147/IJN.S294871.
[41] W.-Q. Chen, W.-J. Wu, Y.-Q. Yu, Y. Liu, F.-L. Jiang, New insights on the size-dependent inhibition of enzymes by gold nanoparticles, Langmuir 39 (2023) 9595–9603, https://doi.org/10.1021/acs.langmuir.3c01367.
[42] S. Alarifi, D. Ali, S. Alkahtani, M.S. Alhader, Iron oxide nanoparticles induce oxidative stress, DNA damage, and caspase activation in the human breast cancer cell line, Biol. Trace Elem. Res. 159 (2014) 416–424, https://doi.org/10.1007/s12011-014-9972-0.
[43] M. Ahamed, H.A. Alhadlaq, J. Alam, M.A. Majeed Khan, D. Ali, S. Alarafi, Iron oxide nanoparticle-induced oxidative stress and genotoxicity in human skin epithelial and lung epithelial cell lines, Curr. Pharmaceut. Des. 19 (2013) 6681–6690, https://doi.org/10.2174/1381612811319370011.
[44] Y. Yang, Y. Qu, X. Lü, Global gene expression analysis of the effects of gold nanoparticles on human dermal fibroblasts, J. Biomed. Nanotechnol. 6 (2010) 234–246, https://doi.org/10.1166/jbn.2010.1128.